Chapter 19

Towards a Self-Deploying and Gliding Robot

Mirko Kovač, Jean-Christophe Zufferey, and Dario Floreano

Abstract Strategies for hybrid locomotion such as jumping and gliding are used in nature by many different animals for traveling over rough terrain. This combination of locomotion modes also allows small robots to overcome relatively large obstacles at a minimal energetic cost compared to wheeled or flying robots. In this chapter we describe the development of a novel palm-sized robot of 10 g that is able to autonomously deploy itself from ground or walls, open its wings, recover in mid-air, and subsequently perform goal-directed gliding. In particular, we focus on the subsystems that will in the future be integrated such as a 1.5 g microglider that can perform phototaxis; a 4.5 g, bat-inspired, wing-folding mechanism that can unfold in only 50 ms; and a locust-inspired, 7 g robot that can jump more than 27 times its own height. We also review the relevance of jumping and gliding for living and robotic systems and we highlight future directions for the realization of a fully integrated robot.

19.1 Introduction

Small robots face big problems when it comes to locomotion in natural and rough terrain. This is usually referred as the "Size Grain Hypothesis" [26], which is described as an "increase in environmental rugosity with decreasing body size." In the animal kingdom, there are many animal species that master locomotion in rough terrain very well by using a combination of different locomotion modes, such as jumping and subsequent gliding flight. This allows them to minimize energetic cost of transport, overcome large obstacles, escape predators, and reduce the potentially hazardous impact forces on landing.

Examples of animals that combine self-deployment with gliding can be found in many different species with different evolutionary origins. Gliding lizards [41, 37, 36, 31], locusts [45], flying fish [17, 5], gliding geckoes [25, 59], gliding ants and spiders [57, 58, 50, 16], gliding squid [32, 5] gliding frogs [35, 20], bats [52], gliding mammals [38, 42, 7, 15], gliding snakes [48, 47] and many birds use combinations of jumps and gliding flight. Gliding can also be found amongst extinct animal species such as the *Sharovipteryx* and some lizard-like reptiles with similar wings to the *Draco* lizard.

It also has been argued [19, 18, 34, 10] that gliding may have been the precursor to flapping flight in insects and vertebrates due to its simplicity.

As the focus of this chapter is of technological nature, the reader may be referred to [51, 18, 5, 40] for in-depth reviews of self-deploying and gliding animals with detailed description of morphology and behavior. Important here to mention, however, is that these animals barely use steady-state gliding, but change their velocity and angle of attack dynamically during flight. This increases the gliding ratio, which is defined as the horizontal distance traveled per unit height loss, or allows the animal to precisely land on a spot, such as perching on a tree branch.

The combination of jumping and gliding is also interesting for miniature robots because it allows them to overcome larger obstacles compared to wheeled and

M. Kovač (✉)
Laboratory of Intelligent Systems, EPFL, Lausanne, Switzerland
e-mail: Mirko.Kovac@epfl.ch

D. Floreano et al. (eds.), *Flying Insects and Robots*,
DOI 10.1007/978-3-540-89393-6_19,

legged robots at the same scale and because it requires less energy compared to flying robots of similar size. In this chapter, we describe our project on the development of a palm-sized microglider of around 10 g that possesses the ability to autonomously self-deploy from ground or walls, open its wings, recover from any position in mid-air, and perform goal-directed gliding.

To date, there have been very few attempts to build robots that combine terrestrial and aerial locomotion.

Armour et al. [4] recently presented a 700 g jumping robot of octahedral shape with wing-like structures to reduce the impact force on landing. This design is able to clear heights of up to 1.17 m but the addition of the wings actually reduces the range of the jump instead of extending it.

A related project with similar aims is the so-called long-jumping "Grillo" mini robot [46]. Prototypes presented so far range in mass between 8 and 80 g and can jump obstacles of approximately 5 cm in height.

Another recent development which is also described in Chap. 18 of this book is a hybrid sensory platform [8] that can crawl using "whegs," a combination of wheels and legs, fold its wings to enter narrow spaces, and perform propelled flight after dropping down from roofs. Its weight is approximately 100 g, with a wingspan of 30.5 cm. It possesses flexible wings as a passive damping mechanism to deal with wind gust, but no quantitative characterization of its efficiency has been presented so far. A limitation of this flying platform is its relatively high weight per unit wing area which necessitates 6.6 m height loss for recovery after dropping down from roofs for the transition to propelled flight. To date, this transition has been shown only when the airplane is dropped along the major axis of the fuselage.

Summarizing, only a few projects address the importance of hybrid locomotion as an efficient way of moving in rough terrain, and none has yet successfully integrated jumping and gliding to overcome large obstacles and reduce the energetic cost of transport.

In the following sections we will present our first steps toward the creation of a self-deploying microglider. We start by outlining miniaturization and efficiency of gliding and the development of a gliding robot. We then proceed to investigate mechanisms for wing folding and rapid deployment, describe the prototype of a jumping microrobot, and conclude with a discussion of how to integrate it with the gliding system.

19.2 Gliding in Robotics

Wood et al. recently presented a remarkable 2.2 g microglider [56] that has been specifically designed for gliding flight. It uses a four-bar piezo actuator for rudder deflection and is intended to avoid obstacles using optical flow. Although this realization is a masterpiece of micromechatronics, no characterization of autonomous flight control has been provided so far. Its relatively high flight velocity of more than 5 m/s largely limits its applicability in tight environments as it requires a turning radius of 8 m to perform a U-turn [21].

As a first step toward our self-deploying microglider, we developed a 1.5 g gliding robot [29] (Fig. 19.1) that can perform phototaxis, similar to the ground vehicles as proposed by Breitenberg [9]. To the best of our knowledge, this microglider is the lightest autonomously flying system to date. In order to achieve this very low weight, we opted for a relatively new kind of steering system. We developed a 0.2 g shape memory alloy (SMA) actuator that is harmoniously integrated into the structure of the microglider and allows for direct control of the rudder. As for navigation, two

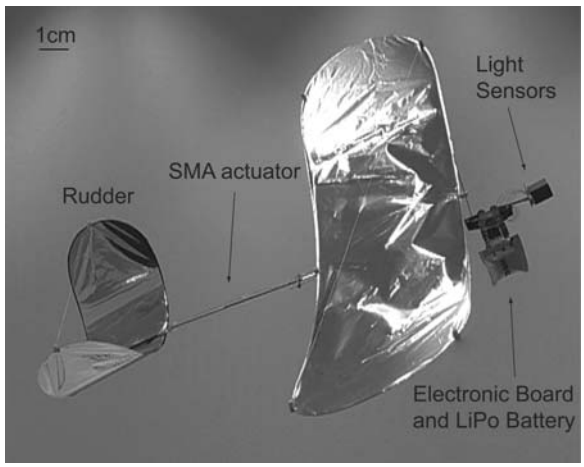

Fig. 19.1 1.5 g SMA-actuated microglider performing autonomous phototaxis with a wingspan of 24 cm, a length of 22 cm, capable of flying at 1.5 m/s

tiny photoreceptors and a simple control strategy were used to detect and follow light gradients.

19.2.1 Airframe, Sensing, and Actuation

The goal of the mechanical airframe design is to reduce the weight as far as possible while keeping the structure simple and easy to produce. As in our indoor flying robots [60], also described in Chap. 6 of this book, we chose to use carbon fiber material for the fuselage, the wing frame, and the rudder (Fig. 19.2). The material of the wing surface is biaxially oriented poly ethylene terephthalate (boPET) film (trade name "Mylar foil") chosen for its high tensile strength. This construction principle leads to an airframe weight of only 0.31 g and has the advantage of being slightly flexible and thus being able to better absorb landing impact forces without breaking. A complete overview of the weight budget is shown in Table 19.1.

Table 19.1 Weight budget of the microglider

Part	Mass (g)
Electronic board	0.33
Battery 10 mAh	0.55
Fuselage	0.18
Front wing	0.1
Rudder	0.03
Light sensors	0.1
SMA actuator	0.2
Cables and soldering	0.02
Total mass	**1.51**

As for the actuation system, different designs and materials could potentially be employed for actuating the control surfaces, such as magnetic coils, piezo actuators, or SMAs. Table 19.2 compares three types of actuators used on airplanes of less than 10 g.

Small magnetic coils are easily available on the market, but deliver comparatively smaller forces and are difficult to control precisely in position. Piezo materials, on the other hand, deliver relatively high forces at very low power consumption, but are limited in displacement and usually require a relatively sophisticated and careful fabrication process and mechanical design. In addition to the actuator itself, the need for relatively heavy electronics to reach the required high voltage (200 V in [56]) decreases the promising properties of this approach for actuation. Therefore, we decided to use thin SMA wires because of their simplicity, high power density, and comparatively large displacement of 5% of their length. For our application of rudder control, we used commercially available nickel titanium alloy (Nitinol) wire, also known as "Muscles Wire" [1].

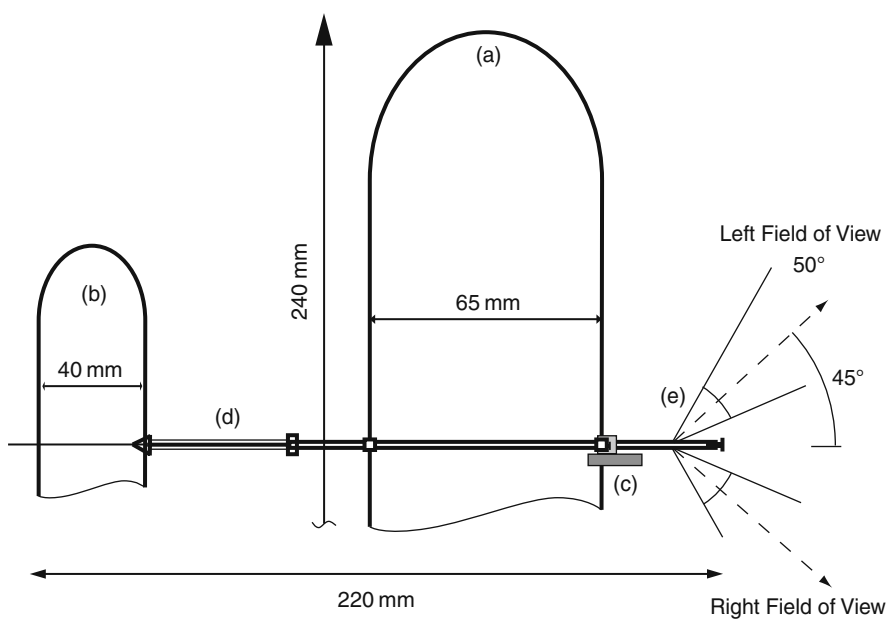

Fig. 19.2 Construction plan of the microglider: (**a**) main wing, (**b**) rudder, (**c**) electronic board and battery, (**d**) SMA actuator, (**e**) light sensors

Table 19.2 Actuator comparison

Actuator type	Mass (g)	Drive electronics (g)	Power (mW)	Commercial availability	Mechanical complexity	Force output
Magnetic coils [2]	0.15	0.02	180	+++	++	-
Piezo [56]	0.05	0.2	7	+	-	+++
SMA [27]	0.12	0.01	171	+	+	++

(+ + + : very favorable; - - - : very unfavorable)

The working principle of SMA wire is that it exploits the crystallographic structure change of martensite to austenite (thermoelastic martensitic transformation) when heated above the transition temperature. This phase change produces a comparatively high force that can be used for actuation. A well-known drawback of SMA in general is its relatively high power consumption. However, for thin wires of 25 μm diameter, the power consumption is only 160 mW, which is comparable to small magnetic actuators.

The actuator we developed consists of (Fig. 19.3a) a copper–beryllium horn (Fig. 19.3e), a 0.7 mm steel tube (Fig. 19.3g), a frame with electrical interface and (Fig. 19.3d), and two 25 μm SMA wires attached to the frame and the horn. The stability of the actuator is given by the carbon fuselage (Fig. 19.3f). The wires are

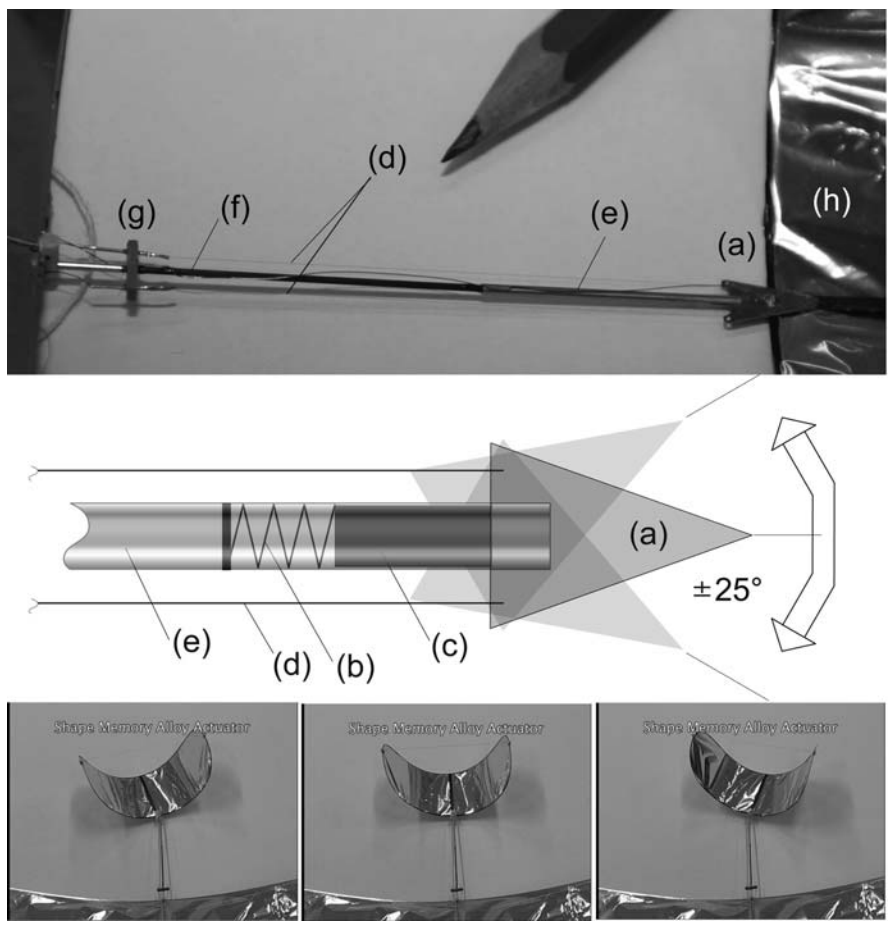

Fig. 19.3 SMA actuator: (**a**) horn, (**b**) spring, (**c**) piston, (**d**) SMA wire, (**e**) steel tube, (**f**) carbon fuselage, (**g**) frame with electrical interface to the electronic board, (**h**) rudder. A PWM signal from the microcontroller heats up the SMA wire on one side. Due to the crystalline structure change this wire contracts and bends the rudder to one side

activated with a pulse width modulation (PWM) signal, which leads to a maximal force of 0.069 N ($\widehat{=}$7 g) at the attachment point of the horn. This leads to a deflection of the horn and of the rudder, which is glued on the horn. The rotation point is the attachment point of the other SMA wire and the counterpart of this movement is the custom-made brass spring (Fig. 19.3b), which ensures back alignment of the rudder to the neutral position at zero PWM duty cycle.

This actuator is then integrated with the airframe, a PIC 16 microcontroller, two light sensors, and a simple proportional control strategy [29], which enables the microglider to autonomously detect and follow light gradients as shown in Fig. 19.4. Launched from a catapult device to provide the glider with a take-off velocity of 2 m/s, it displays a gliding ratio of 5.6, which is relatively high compared to many gliding animals at such small scales. In order to characterize its phototaxis capabilities, we carried out three series of launches, each with a different position of the light bulb, and showed that the glider consistently lands near the light source (Fig. 19.4).

19.2.2 Wing Folding

The technology described above is promising for a small jumping robot, but the fixed open wings offer too much resistance to the air during the deployment phase of the jump. In order to maximize the jump height, the exposed wing surface has to be as small as possible during deployment. We thus aimed at developing a wing-folding mechanism that keeps the wings contracted while the robot is in the deployment phase and quickly unfolds them when the robot starts to lose altitude. The requirements for such a mechanism are to be able to open very quickly, be as lightweight as possible, stable when open, and robust enough to withstand eventual crash landings.

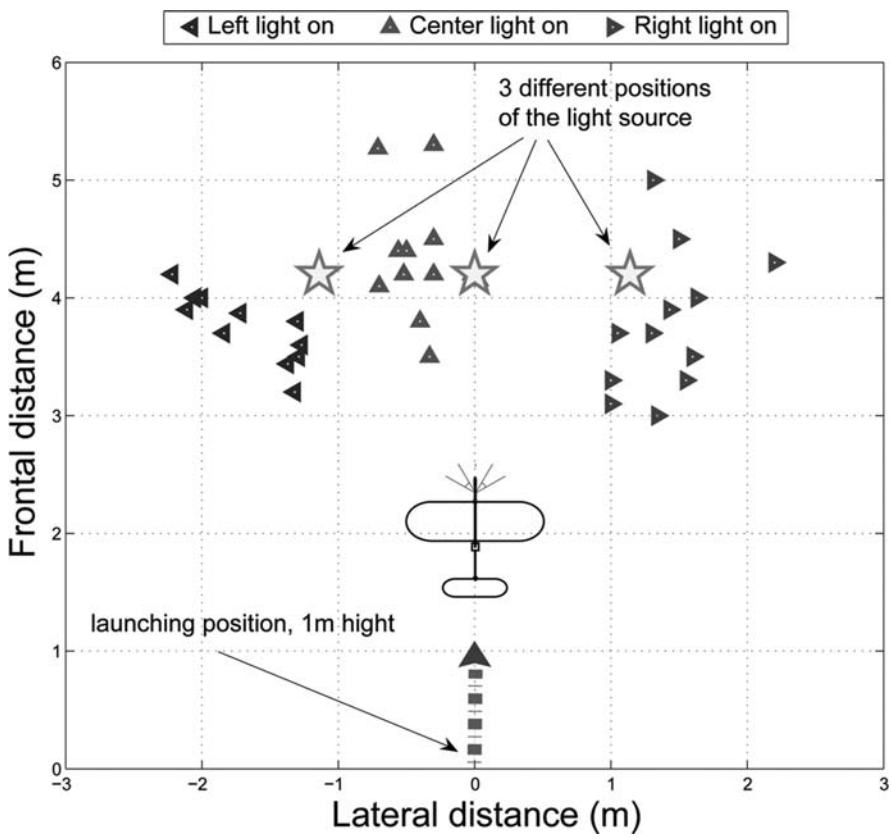

Fig. 19.4 *Top* view of the setup for the phototaxis experiments. Stars indicate the three possible light source locations. For each of the three locations, 12 subsequent launches have been carried out. The triangles mark the landing positions

Nature offers many foldable structures, which are a potential source of inspiration for the design of such a mechanism. For example, leaves unfold from a very compact package to the complete unfolded leaf with a high structural stability [33, 43]. Other ways of unfolding can be found in soft animals, such as anemones and various worms [55, 53]. Also, many insects use origami-like mechanisms to fold their wings, such as the hind wings of *Dermaptera* [23, 24], and most of the birds and bats fold wings to protect their often fragile structures. Figure 19.5 shows some examples of folding structures found in nature.

Origami-like structures are very interesting and when carefully designed would even allow to unfold in a 3D shape and form a cambered wing (similar as the wooden roof structures in [12], see Fig. 19.5). A difficulty for this technology, however, is to find an appropriate material that is light enough and can be used on such small scales. After a detailed evaluation phase of all those solutions and several conceptional prototypes, we decided to adopt an abstracted form of the wing-folding principle used by bats. The main advantages of this solution are its structural stability when open and the possibility to easily build the skeleton out of carbon and cover the wing itself with Mylar foil so as to yield a minimal weight. The realized prototype (Fig. 19.6) weights only 4.5 g and is able to unfold its wings in 50 ms on command using a SMA-based locking mechanism.

The skeleton of the wing-folding mechanism consists of six hinges that are interconnected with 1 mm

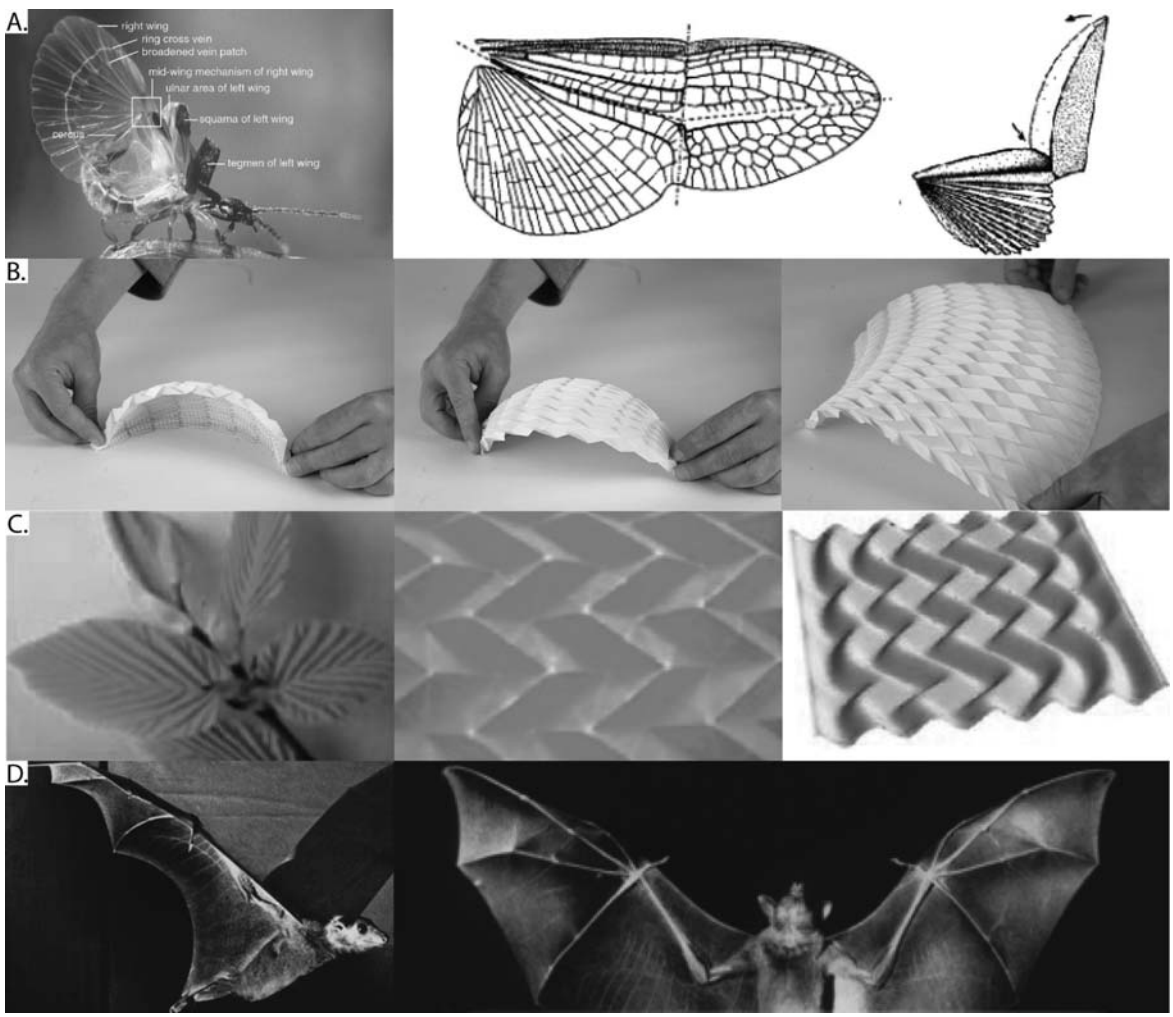

Fig. 19.5 A selection of folding structures: (**A**) hind wings of *Dermaptera* [23, 24]; (**B**) model of a wooden roof structure [12]; (**C**) folding leafs [33]; (**D**) wing folding in bats [39]

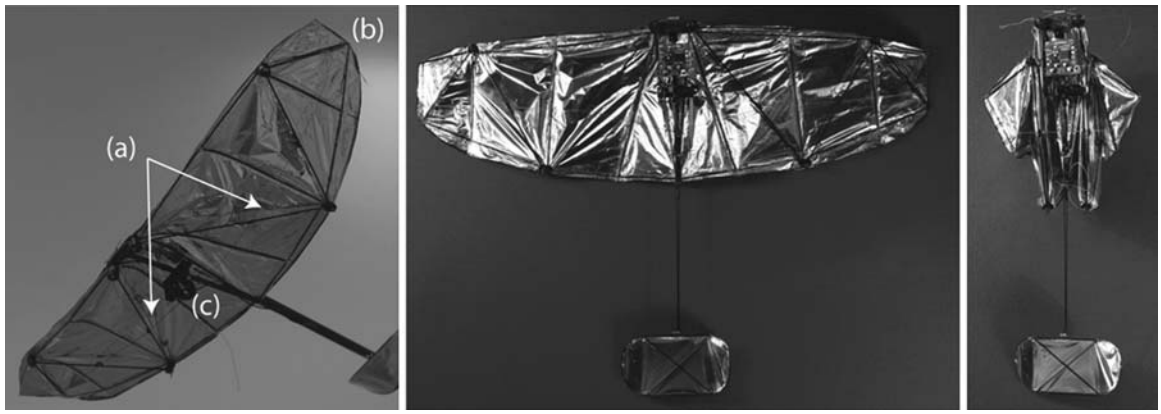

Fig. 19.6 Bat-inspired wing-folding system. A string (**a**) is attached to the wing tips (**b**) and is rolled on a spool (**c**) to fold the wing

carbon rods and covered with aluminum-coated 5 μm Mylar foil (Fig. 19.6). The folding of the wings happens by rolling up a string (a) which is attached at the tip of the wing (b). The hinges contain each a torsion spring that is encapsulated in a polyoxymethylene (POM) frame (Fig. 19.8). By rolling up the string, the torsion springs store elastic energy and unfold the wing once the string gets released. A complete unfolding sequence takes only 50 ms and can be seen in Fig. 19.7. In order to roll up and release the string, we developed a SMA-based unlocking mechanism, which will be described next.

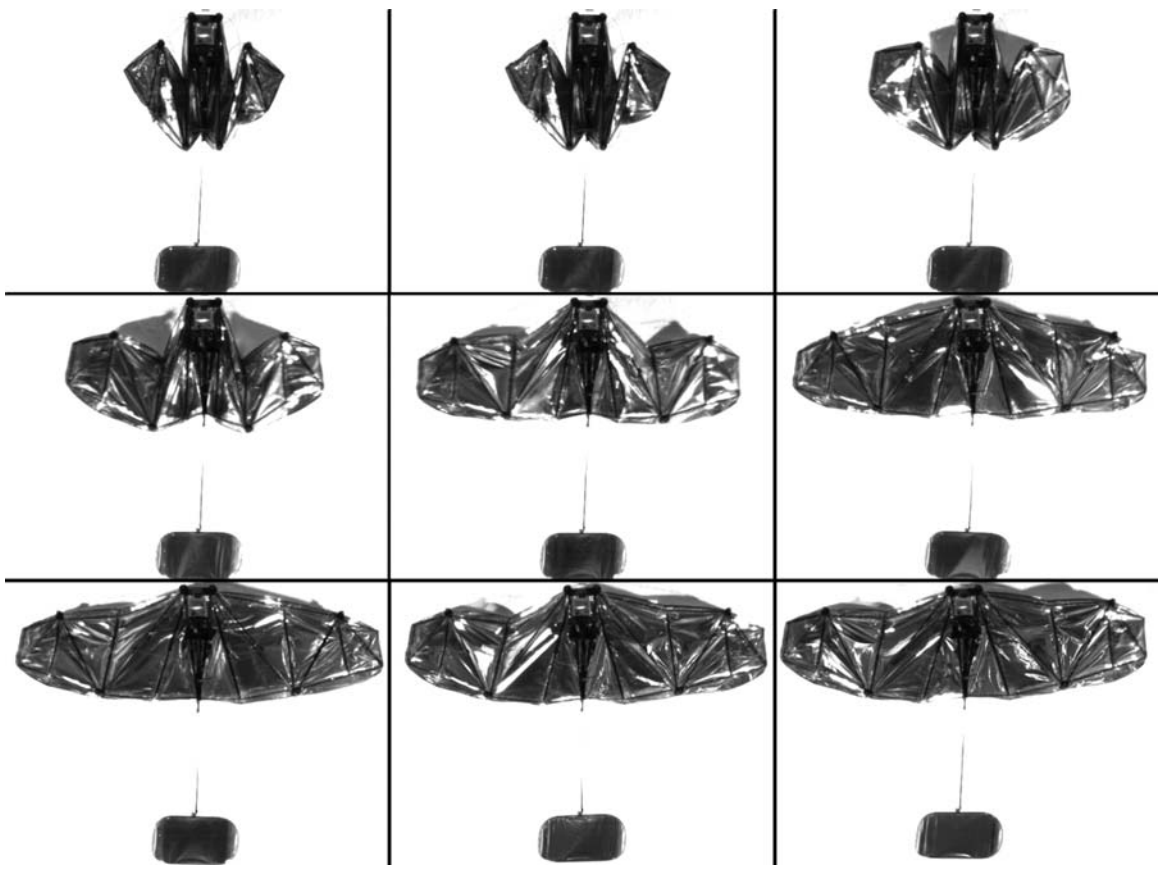

Fig. 19.7 A complete unfolding sequence takes only 50 ms

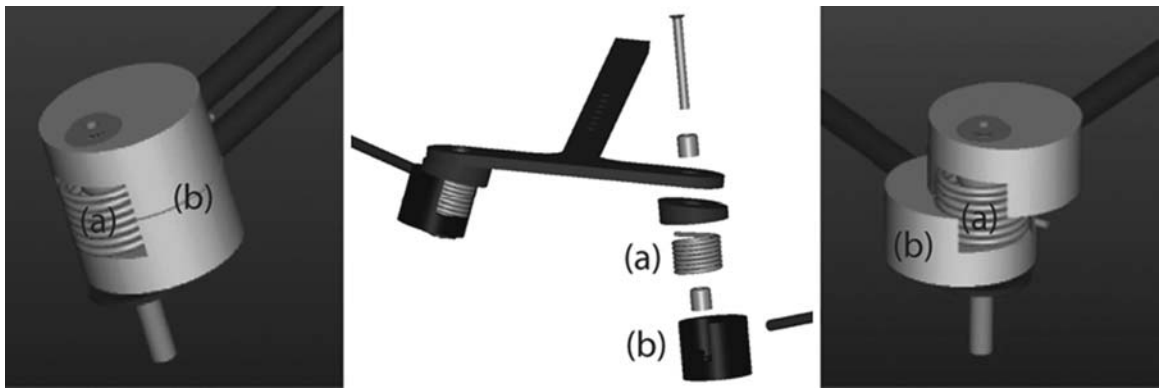

Fig. 19.8 The wing-folding mechanism contains six hinges which are interconnected with carbon rods. The torsion spring (**a**) is embedded in a POM frame (**b**)

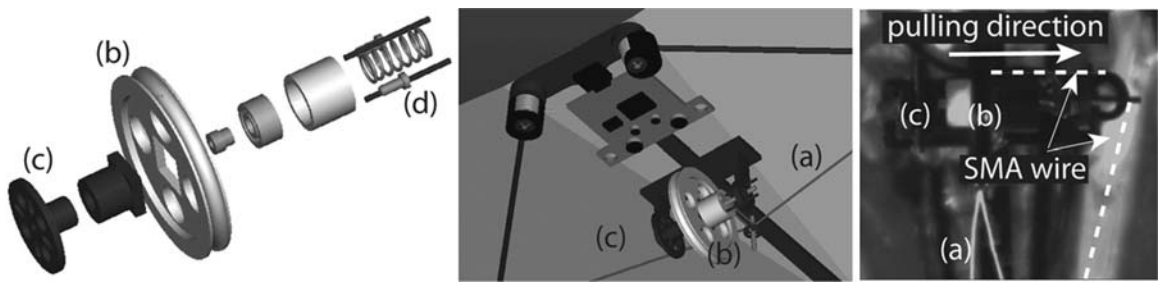

Fig. 19.9 SMA-based release mechanism. The string (**a**) is attached to the wing tip and gets rolled up on the spool (**b**), which is connected to the gear (**c**). A 37 μm SMA wire pulls the spool laterally to unlock it from the gear and to allow the wing to unfold. After relaxing the SMA, the spring (**d**) pushes the spool back and connects it with the gear for the next folding cycle

In order to fold the wing, the string (Fig. 19.9a) that is attached to the wing tip is rolled on the spool (Fig. 19.9b). The spool itself is connected to a gear (Fig. 19.9c) which is interfaced with the gearbox of the jumping mechanism as we will describe later in Sect. 19.4. A 37 μm SMA wire (Fig. 19.9) contracts and pulls the spool laterally, to unlock it from the gear and thus allows the force stored in the torsion springs in the hinges of the wings to unfold the wings. As soon as the unfolding is completed, the spring (Fig. 19.9d) pushes the spool back and reconnects it with the gear (Fig. 19.9c) in order to fix the position and allow the next folding sequence.

19.3 Jumping

The jumping mechanism must be lightweight and capable of propelling the glider as high as possible into the air. Table 19.3 summarizes the performance of existing jumping robots with onboard energy and control. None of these systems are sufficient to meet the weight and size constrains of our self-deploying microglider, i.e., palm sized with an entire system weight of 10 g. We thus developed a 5 cm jumping mechanism [28] (Figs. 19.10, 19.11) weighting a mere 7 g with electronics and battery. It consists of the gearbox including motor, gearwheels and cam, the main leg, carbon rods as feet, the infrared receiver, and a 10 mAh lithium polymer battery. Its design allows to manually adjust the take-off angle, jumping force, and force profile during the acceleration phase. This is useful to obtain a desired trajectory, jumping height, and to be able to optimize jumping on slippery surfaces or compliant substrates.

It has been shown [3, 6, 44] that at small size it is most advantageous to slowly charge an elastic element, release it with a click mechanism, and amplify the take-off velocity using the legs as catapults, rather than applying a squad or countermovement jump. This

Table 19.3 State of the art on jumping robots with onboard energy and control

Name	Mass [g]	Approx. jump height [cm]	Jump height per mass [cm/g]	Approx. jump height per size [-]
Rescue robot [54]	2000	80	0.04	3.5
Minimalist jumping robot [11]	1300	90	0.07	6
Jollbot [4]	465	21.8	0.05	1.4
Glumper [4]	700	50	0.23	3.2
Scout [49]	200	35	0.18	3.5
Mini-Whegs [30]	190	22	0.12	2.2
Grillo [46]	8–80	5	0.63–0.06	1
Jumping robot presented here	**7**	**138**	**19.77**	**27.6**

Fig. 19.10 A 7 g jumping robot prototype capable of clearing obstacles of up to 1.4 m height along with a desert locust using the same biomechanical design principle for jumping

principle is used by most of the small jumping animals such as frogs [44], desert locusts [6], stick insects [14], froghoppers [13], click beetles [3], or fleas [22]. We applied the same biomechanical design principles and were capable of achieving a very high jumping performance compared to existing jumping robots (Table 19.3).

By changing the proportions of the four-bar leg mechanism (Fig. 19.12) we can generate different foot tip trajectories, which translates to different ground force profiles, acceleration times, and take-off angles depending on which length is changed. The amount of energy that will be stored in the springs can be adjusted between 106 and 154 mJ in steps of 6 mJ, by changing the spring setting (Fig. 19.11f). The two body plates (Fig. 19.11g) consist of a material called Cibatool, which is commonly used for rapid prototyping, can be easily machined, and has low weight. The cam and gears are manufactured from polyoxymethylene (POM) due to its low weight and low surface friction

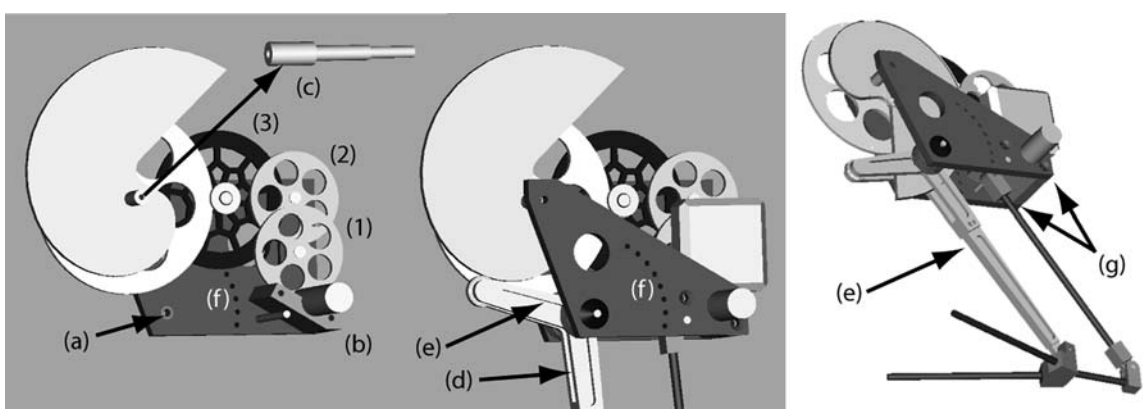

Fig. 19.11 CAD model of the gearbox: (**a**) brass bearing to reduce friction, (**b**) distance piece to align the two body plates, (**c**) cam axis, (**d**) slot in main leg for the cam, (**e**) main leg, (**f**) series of holes for spring setting, and (**g**) the two body plates. (1), (2) 0.2 mm polyoxymethylene (POM) gears and (3) 0.3 mm POM gear

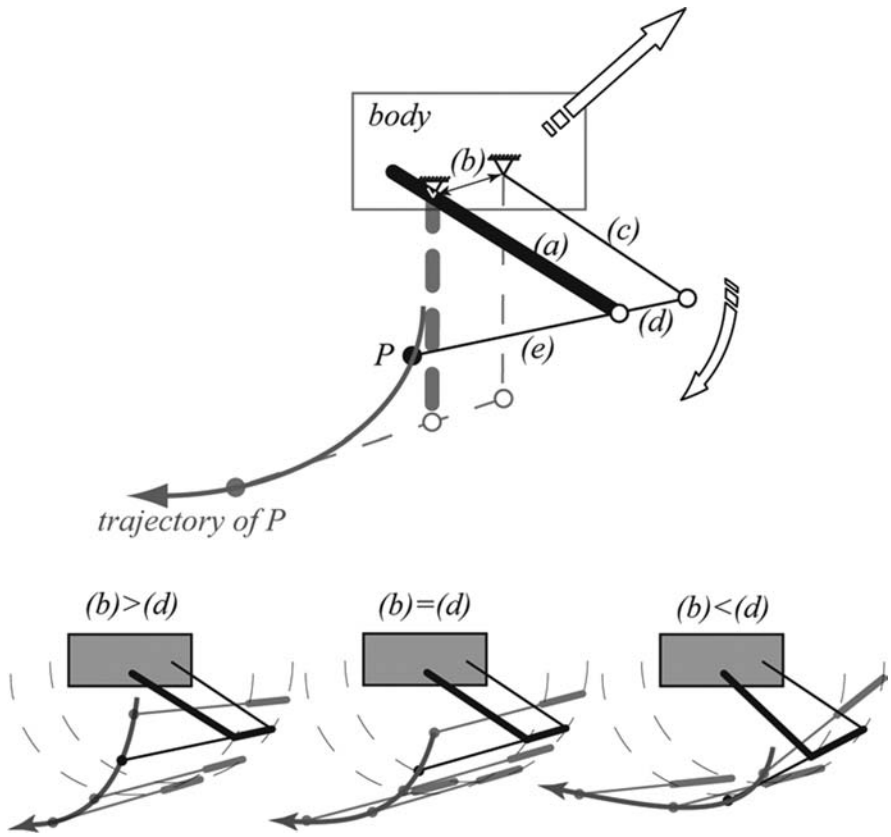

Fig. 19.12 Sketch of the four-bar linkage jumping design and the foot tip P trajectory during takeoff: (a) the input link and (b) the ground link. Changing the length of these four bars allows to adjust the take-off angle (change distance (e)), acceleration time (change distance (a) and (c)), and trajectory of the foot tip P (change ratio (b)/(d))

coefficient. For critical structural parts in the body and legs we used polyetheretherketone (PEEK) due to its very high strength-to-weight ratio. Table 19.4 presents the weight budget of the robot. The entire and fully functional remote-controlled prototype weights 6.98 g in its current form. Further weight reduction could be achieved by optimizing the two body plates, e.g., by drilling additional holes in it and by using a smaller infrared receiver and battery.

Figure 19.13 depicts a complete take-off sequence of the jumping prototype including a payload of 3 g on top of the 7 g prototype. In order to illustrate the adaptability of the jumping force, Fig. 19.14 shows the jumping trajectories that were extracted from high-speed movies for the jumping robot without, and with, a payload of 3 g. The maximal height obtained without additional payload was 138 cm. The acceleration time was 15 ms, the initial take-off velocity 5.96 m/s, and the velocity at the top 0.9 m/s. The complete jump

Table 19.4 Weight budget of the jumping robot

Part	Material	Weight [g]
Body frame	Cibatool/PEEK	1.4
Cam	POM	0.78
Gears	POM	0.63
Main leg	Aluminium	0.76
Plastic parts on leg	PEEK/Carbon	0.32
Screws and axis	Steel/brass	0.79
Two springs	Spring steel	0.41
Motor		0.65
Total mass mechanism		**5.74**
LiPo Battery		0.48
IR receiver		0.76
Total mass prototype		**6.98**

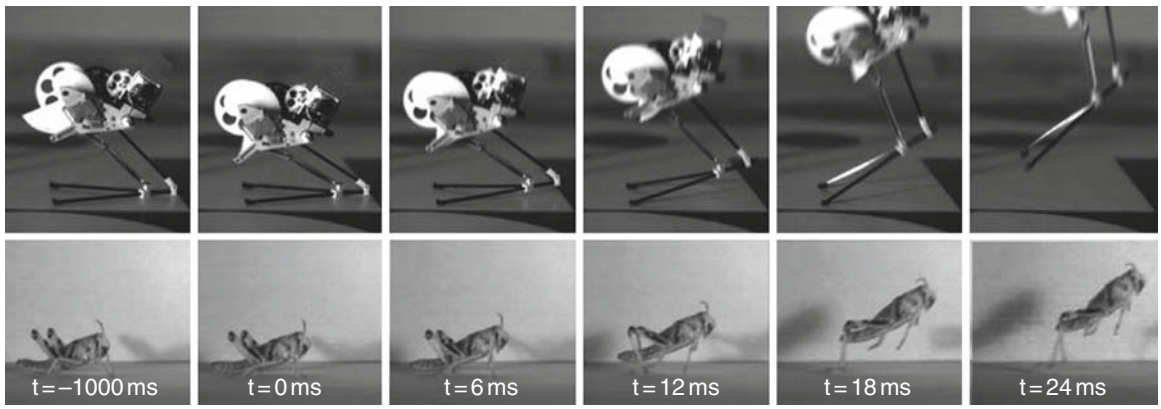

Fig. 19.13 Take-off sequence of our jumping robot compared to a desert locust

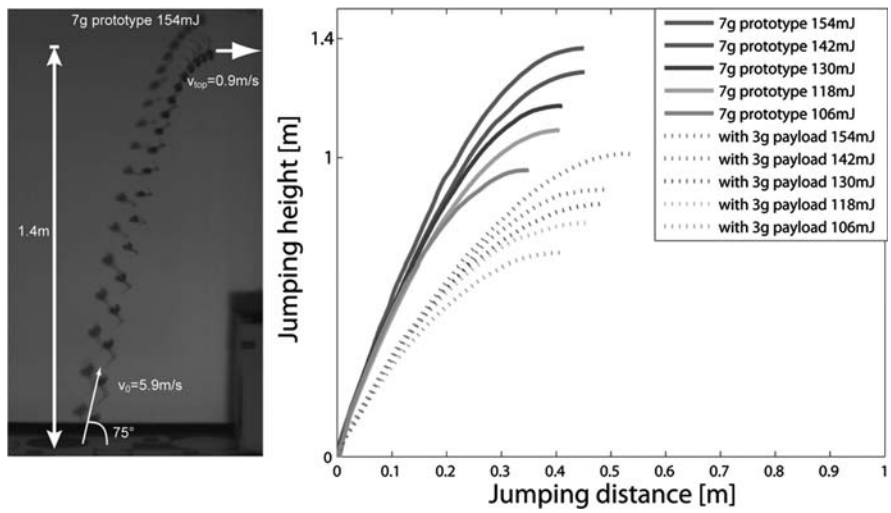

Fig. 19.14 Jump trajectory at different spring settings for the prototype with and without an additional payload of 3 g

duration is 1.02 s and the traveled distance 79 cm at a take-off angle of 75°. This means that the prototype presented here is capable of overcoming obstacles of more than 27 times its own body size.

The motor recharges the mechanism for one jump cycle in 3.5 s. Using a 0.48 g LiPo battery, it thus allows for approximately 108 jumps.

19.4 System Integration

The next step is to combine the jumping mechanism with the wing-folding system in order to allow the robot to jump and unfold the wings at the top of the jumping trajectory. This, however, poses a number of integration challenges related to actuation and dynamics of the complete system. Figure 19.15 depicts a CAD model of a possible integration of the two mechanism. The gear (Fig. 19.9c and 19.15a) from the wing-folding mechanism is interfaced with the third stage of the gear systems of the jumping mechanism (Figs. 19.11, 19.3, 19.15b). While charging the legs for jumping, this coupled system folds also the wings. Once the robot takes off, the wings are opened by the SMA-based release mechanism as described in Sect. 19.2.2. Here, an important challenge is to define the time to unfold the wings. Since the forces acting on the system are very small at the top of the jump trajectory, it is difficult to precisely determine when it is best

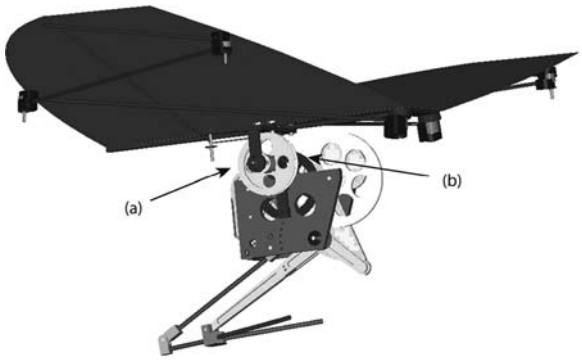

Fig. 19.15 CAD model of a possible integration of the subsystems. The gear from the wing-folding mechanism (**a**) is interfaced with the third stage of the gear system of the jumping mechanism (**b**). While charging the legs for jumping, it also folds the wings which it can release on command on top of the jumping trajectory

to unfold the wings. A possible solution may be to just assume a time constant when to open the wings after takeoff. However, this integration of the wing-folding and the jumping mechanism still has the limitation that the attitude of the glider on top of the jump has to be upright in order to permit the robot to recover and perform stable gliding flight. Future work addresses the question how to recover from any position in air and ensure a proper transition to the subsequent gliding phase.

19.5 Conclusion

In this chapter, we highlighted jumping and gliding as a promising locomotion strategy to move across rough terrain. Although there still remain challenges in the integration of the components that a self-deploying microglider will need, the three subsystems described here may also be used as stand-alone platforms. For example, the jumping prototype could be equipped with an uprighting mechanism, a small communication unit, and sensors such as cameras or chemical sensors to perform environmental or security monitoring. The gliding system may also be equipped with sensors and launched from the roof of buildings or from airplanes to monitor the environment. The wing-folding mechanism may allow the robot to be thrown high in the air by hand or by a catapult system.

Biological systems were a useful source of inspiration; for example, the wing-folding mechanism adopts the mechanical principle from bats to fold the wings, which leads to a very lightweight, simple, and stable wing-folding mechanism. Another example of direct biological inspiration is the jumping robot which, in the same way as, e.g., locusts or fleas, first slowly charges an elastic element in the legs and then releases it quickly using a click mechanism to perform a catapult jump. On the other hand, such a robot may also be used as a physical model to test models of jumping and gliding in nature. The parameters that can be adjusted in our robotic platform include (i) the mass, (ii) the strength of the motor and spring in the jumping mechanism, (iii) the ground force profile during the acceleration phase of jumping, (iv) the leg length and flexibility, (v) the wing size and shape, and (vi) the coordination between the jumping and wing-folding subsystems, e.g., when to open the wings and how to stabilize and recover. By modifying these parameters, scale effects, such as the interplay between mass and size, of jumping animals can be investigated. The way in which the addition of wings affects jumping performance and the distance traveled per energy unit may also give insight in the evolution of flight.

Acknowledgments The authors would like to thank Martin Fuchs and Gregory Savioz for their significant contribution in the development of the wing-folding mechanism and the jumping robot. Also we would like to thank the Atelier de l'Institut de production et Robotique (ATPR), and André Guignard for their competent advice and endurance in the iterative fabrication process. Many thanks to Hans Ulrich Buri at EPFL for the fruitful discussion and advise on the Origami structures. This project is funded by EPFL and by the Swiss National Science Foundation, Grant number 200021-105545/1.

References

1. Info-sheet No. 13, Nitinol Alloy Types, Conditions and Surfaces. http://www.memory-metalle.de
2. Micro flyer radio. http://www.microflierradio.com
3. Alexander, R.M.: Principles of Animal Locomotion. Princeton University Press (2003)
4. Armour, R., Paskins, K., Bowyer, A., Vincent, J.F.V., Megill, W.: Jumping robots: a biomimetic solution to locomotion across rough terrain. Bioinspiratoin and Biomimetics Journal **2**, 65–82 (2007)
5. Azuma, A.: The Biokinetics of Flying and Swimming. American Institute of Aeronautics and Astronautics (2006)

6. Bennet-Clark, H.C.: The energetics of the jump of the locust schistocerca gregaria. Journal of Experimental Biology **63**(1), 53–83 (1975)
7. Bishop, K.L.: The relationship between 3-d kinematics and gliding performance in the southern flying squirrel, glaucomys volans. Journal of Experimental Biology **209**(4), 689–701 (2006)
8. Boria, F.J., Bachmann, R.J., Ifju, P., Quinn, R., Vaidyanathan, R., Perry, C., Wagener, J.: A sensor platform capable of aerial and terrestrial locomotion. 2005 IEEE/RSJ International Conference on Intelligent Robots and Systems, 2005. (IROS 2005), pp. 3959–3964 (2005)
9. Braitenberg, V.: Vehicles – Experiments In Synthetic Psychology. The MIT Press, Cambridge, MA (1984)
10. Brodsky, A.K.: The Evolution of Insect Flight. Oxford University Press (1996)
11. Burdick, J., Fiorini, P.: Minimalist jumping robot for celestial exploration. The International Journal of Robotics Research **22**(7), 653–674 (2003)
12. Buri, H., Weinand, Y.: ORIGAMI - folded plate structures, architecture. 10th World Conference on Timber Engineering (2008)
13. Burrows, M.: Biomechanics: Froghopper insects leap to new heights. Nature **424**(6948), 509
14. Burrows, M., Wolf, H.: Jumping and kicking in the false stick insect prosarthria teretrirostris: kinematics and motor control. Journal of Experimental Biology **205**(11), 1519–1530 (2002)
15. Byrnes, G., Lim, N., Spence, A.: Take-off and landing kinetics of a free-ranging gliding mammal, the malayan colugo (galeopterus variegatus) (2008)
16. Coyle, F.A., Greenstone, M.H., Hultsch, A.L., Morgan, C.E.: Ballooning mygalomorphs: Estimates of the masses of sphodros and ummidia ballooners(araneae: Atypidae, ctenizidae). Journal of Arachnology **13**(3), 291–296 (1985)
17. Davenport, J.: Allometric constraints on stability and maximum size in flying fishes: Implications for their evolution. Journal of Fish Biology **62**, 455–463 (2003)
18. Dudley, R., Byrnes, G., Yanoviak, S.P., Borrell, B., Brown, R.M., McGuire, J.A.: Gliding and the functional origins of flight: Biomechanical novelty or necessity? Annual Review of Ecology Evolution and System **38**, 179–201 (2007)
19. Dyke, G.J., Nudds, R.L., Rayner, J.M.V.: Flight of sharovipteryx mirabilis: the world's first delta-winged glider. Journal of Evolutionary Biology **19**(4), 1040–1043 (2006)
20. Emerson, S.B., Koehl, M.A.R.: The interaction of behavioral and morphological change in the evolution of a novel locomotor type: "flying" frogs. Evolution **44**(8), 1931–1946 (1990)
21. Entwistle, J.P., Fearing, R.S.: Flight simulation of a 3 gram autonomous glider, available at http://www.stormingmedia.us/16/1693/A169374.html (2006)
22. Gronenberg, W.: Fast actions in small animals: springs and click mechanisms. Journal of Comparative Physiology A: Sensory, Neural, and Behavioral Physiology **178**(6), 727–734 (1996)
23. Haas, F., Gorb, S., Wootton, R.J.: Elastic joints in dermapteran hind wings: materials and wing folding. Arthropod Structure and Development **29**(2), 137–146 (2000)
24. Haas, F., Wootton, R.J.: Two basic mechanisms in insect wing folding. Proceedings: Biological Sciences **263**(1377), 1651–1658 (1996)
25. Jusufi, A., Goldman, D.I., Revzen, S., Full, R.J.: Active tails enhance arboreal acrobatics in geckos. Proceedings of the National Academy of Sciences **105**(11), 4215–4219 (2008)
26. Kaspari, M., Weiser, M.D.: The sizegrain hypothesis and interspecific scaling in ants. Functional Ecology **13**(4), 530–538 (1999)
27. Keennon, M.T.: Muscle Wire Technology for Micro and Indoor Models (2004)
28. Kovac, M., Fuchs, M., Guignard, A., Zufferey, J., Floreano, D.: A miniature 7 g jumping robot (2008)
29. Kovac, M., Guignard, A., Nicoud, J.D., Zufferey, J.C., Floreano, D.: A 1.5 g sma-actuated microglider looking for the light. IEEE International Conference on Robotics and Automation, pp. 367–372 (2007)
30. Lambrecht, B.G.A., Horchler, A.D., Quinn, R.D.: A small, insect-inspired robot that runs and jumps. International Conference on Robotics and Automation, pp. 1240–1245 (2005)
31. Li, P.P., Gao, K.Q., Hou, L.H., Xu, X.: A gliding lizard from the early cretaceous of china. Proceedings of the National Academy of Sciences **104**(13), 5507 (2007)
32. Macia, S., Robinson, M.P., Craze, P., Dalton, R., Thomas, J.D.: New observations on airborne jet propulsion (flight) in squid, with a review of previous reports (2004)
33. Mahadevan, L., Rica, S.: Self-organized origami. Science **307**(5716), 1740 (2005). 10.1126/science.1105169. http://www.sciencemag.org/cgi/content/abstract/307/5716/1740
34. Maynard Smith, J.: The importance of the nervous system in the evolution of animal flight. Evolution **6**(1), 127–129 (1952)
35. McCay, M.G.: Aerodynamical stability and maneuvrability of the gliding frog polypedates dennysi. Journal of Experimental Biology **204**, 2817–2826 (2001)
36. McGuire, J.A.: Allometric prediction of locomotor performance: An example from southeast asian flying lizards. The American Naturalist **161**(2), 337–9
37. McGuire, J.A., Dudley, R.: The cost of living large: Comparative gliding performance in flying lizards (agamidae: Draco). The American Naturalist **166**(1), 93–106 (2005)
38. Meng, J., Hu, Y., Wang, Y., Wang, X., Li, C.: A mesozoic gliding mammal from northeastern china. Nature **444**, 889–893
39. Norberg, U.M.: Bat wing structures important for aerodynamics and rigidity (mammalia, chiroptera). Zoomorphology **73**(1), 45–61 (1972)
40. Norberg, U.M.: Vertebrate Flight: Mechanics, Physiology, Morphology, Ecology and Evolution (1990)
41. Oliver, J.A.: "gliding" in amphibians and reptiles, with a remark on an arboreal adaptation in the lizard, anolis carolinensis carolinensis voigt. The American Naturalist **85**(822), 171–176 (1951). http://www.jstor.org/stable/2457833
42. Paskins, K.E., Bowyer, A., Megill, W.M., Scheibe, J.S.: Take-off and landing forces and the evolution of controlled gliding in northern flying squirrels glaucomys sabrinus. Journal of Experimental Biology **210**(8), 1413 (2007)
43. Pellegrino, S.: Deployable Structures (2002)

44. Roberts, T.J., Marsh, R.L.: Probing the limits to muscle-powered accelerations: lessons from jumping bullfrogs. Journal of Experimental Biology **206**(15), 2567–2580 (2003)
45. Santer, R., Simmons, P., Rind, F.C.: Gliding Behaviour Elicited by Lateral Looming Stimuli in Flying Locusts. Journal of Comparative Physiology **191**(1), 61–73 (2004)
46. Scarfogliero, U., Stefanini, C., Dario, P.: Design and development of the long-jumping "grillo" mini robot. IEEE International Conference on Robotics and Automation, pp. 467–472 (2007)
47. Socha, J., LaBarbera, M.: Effects of Size and Behavior on Aerial Performance of two Species of Flying Snakes (Chrysopelea). The Journal of Experimental Biology **208**, 1835–1847 (2005)
48. Socha, J., O'Dempsey, T., LaBarbera, M.: A 3-d kinematic analysis of gliding in a flying snake, chrysopelea paradisi. Journal of Experimental Biology **208**(10), 1817–1833 (2005)
49. Stoeter, S.A., Rybski, P.E., Papanikolopoulos, N.: Autonomous stair-hopping with scout robots. IEEE/RSJ International Conference on Intelligent Robots and Systems, vol.1, pp. 721–726 (2002)
50. Suter, R.B.: Ballooning: data from spiders in freefall indicate the importance of posture. Journal of Arachnology **20**(2), 107–113 (1992)
51. Templin, R.J.: The spectrum of animal flight: insects to pterosaurs. Progress in Aerospace Sciences **36**(5–6), 393–436 (2000)
52. Thomas, A.L.R., Jones, G., Rayner, J.M.V., Hughes, P.M.: Intermittent gliding flight in the pipistrelle bat (pipistrellus pipistrellus)(chiroptera: Vespertilionidae). Journal of Experimental Biology **149**(1), 407–416 (1990)
53. Thompson, D.: On growth and form (1992)
54. Tsukagoshi, H., Sasaki, M., Kitagawa, A., Tanaka, T.: Design of a higher jumping rescue robot with the optimized pneumatic drive. IEEE International Conference on Robotics and Automation, pp. 1276–1283 (2005)
55. Vincent, J.F.V.: Deployable Structures in Biology, pp. 23–40. Springer (2003)
56. Wood, R., Avadhanula, S., Steltz, E., Seeman, M., Entwistle, J., Bachrach, A., Barrows, G., Sanders, S., Fearing, R.: Design, fabrication and initial results of a 2 g autonomous glider. IEEE Industrial Electronics Society 2005 Meeting, Raleigh North Carolina (2005)
57. Yanoviak, S., Dudley, R., Kaspari, M.: Directed Aerial Descent in Canopy Ants. Nature **433**, 624–626 (2005)
58. Yanoviak, S.P., Dudley, R.: The role of visual cues in directed aerial descent of cephalotes atratus workers (hymenoptera: Formicidae). Journal of Experimental Biology **209**(9), 1777–1783 (2006)
59. Young, B.A., Lee, C.E., Daley, K.M.: On a flap and a foot: Aerial locomotion in the "flying" gecko, ptychozoon kuhli. Journal of Herpetology **36**(3), 412–418 (2002)
60. Zufferey, J.C., Floreano, D.: Fly-inspired visual steering of an ultralight indoor aircraft. IEEE Transactions on Robotics **22**, 137–146 (2006)